Limnol. Oceanogr., 43(5), 1998, 769–781

Dissolved inorganic carbon profiles and fluxes determined using pH and P_{CO_2} microelectrodes

Tomoko Komada, Clare E. Reimers, and Susan E. Boehme
Institute of Marine and Coastal Sciences, Rutgers, The State University of New Jersey, New Brunswick, New Jersey 08901-8521

Abstract

Submillimeter depth distributions of total dissolved inorganic carbon (DIC) were derived from pH and P_{CO_2} profiles measured with microelectrodes in an organic-rich, laboratory-maintained sediment. The DIC profiles were used to calculate diffusive fluxes of DIC across the sediment–water interface. In two experiments, the calculated diffusive fluxes fell within ±50% of the total flux of DIC determined by core incubation. An assessment of errors suggests that the microelectrode-derived estimates are not significantly different from measured total DIC fluxes ($P = 0.05$). It is concluded, therefore, that pH and P_{CO_2} microelectrode measurements can be paired to determine fine-scale pore-water DIC profiles and DIC diffusive fluxes. Problems will arise only in situations in which pH and P_{CO_2} gradients are extremely steep or spatially heterogeneous; this is because these conditions can cause mismatching of pH and P_{CO_2} measurements or CO_2 system disequilibrium.

Microelectrodes have been used to measure in situ oxygen and pH pore-water profiles in a wide variety of marine environments in recent years. These new data are being used to calculate diffusive benthic fluxes of O_2 (Reimers et al. 1986, 1992; Archer and Devol 1992; Glud et al. 1994*a*) and applied as constraints for diagenetic models that estimate rates of organic matter degradation and calcium carbonate dissolution (Archer et al. 1989; Cai et al. 1995; Hales and Emerson 1996, 1997). However, one shortcoming of these studies is that O_2 and pH data need to be accompanied by an additional measurable parameter of the CO_2 system to fully describe this system in pore solutions.

P_{CO_2} is the only other parameter of the CO_2 system that is readily measurable by microelectrodes. Therefore, Cai and Reimers (1993) and Cai et al. (1995) attempted to use a potentiometric P_{CO_2} microelectrode to measure the first in situ P_{CO_2} profiles in marine sediments. These P_{CO_2} profiles, however, did not compare well with models constrained by the pH and oxygen microelectrode data at several key depths within the sediment. Cai and Reimers (1993) and Cai et al. (1995) attributed these deviations to the slow response characteristics of the potentiometric P_{CO_2} sensor.

The goal of this study was to verify that potentiometric pH and P_{CO_2} microelectrodes, given adequate response times, produce pH and P_{CO_2} data that can be used to derive (1) reliable total dissolved inorganic carbon (DIC) concentrations in pore waters and (2) accurate DIC fluxes across the sediment–water interface. Diffusive fluxes of DIC across the sediment–water interface were calculated using pH and P_{CO_2} microelectrode profiles and compared with total fluxes determined directly using laboratory core incubations as the primary test of microelectrode performance. It was assumed that gradient-supported fluxes should agree with total fluxes as long as (1) biologically mediated solute transport and significant pore-water advection were absent; (2) DIC production was independent of time; and (3) accurate pore-water gradients, along with the correct diffusivities, were used in the diffusive flux calculations. Intercomparisons of predicted diffusive fluxes and measured total fluxes have been conducted for various dissolved substances, including oxygen, nutrients, DIC, and dissolved organic carbon (McCaffrey et al. 1980; Rutgers van der Loeff et al. 1984; Berelson et al. 1987, 1990; Burdige and Homstead 1994; Boehme et al. 1996), although determination of diffusive fluxes using microelectrodes has been limited to oxygen (Reimers and Smith 1986; Archer and Devol 1992; Rasmussen and Jørgensen 1992; Glud et al. 1994*a*). Fluxes of oxygen predicted from microelectrode gradients have generally shown good agreement with total fluxes in the absence of vigorous bioirrigation (Reimers and Smith 1986; Rasmussen and Jørgensen 1992; Glud et al. 1994*a*; Hales and Emerson 1996), supporting the validity of microgradient-determined benthic fluxes.

Materials and methods

Site description and sample handling—Sediment samples were collected from a tidal inlet at Schooner Creek, Tuckerton, New Jersey, in March and June 1995. These samples were used in two separate experiments, referred to as Exp. 1 and Exp. 2, respectively. The sediments were organic-rich, fine-grained, and anoxic. The sediment surface, which is normally fully exposed to the atmosphere during low tide, was covered with patches of microbial mat.

Sediment cores were collected for both experiments using an acrylic flux chamber (Fig. 1). The core tube was inserted into the sediment so that the water column was ~10 cm high. The cores were transported back to the laboratory, where they were allowed to equilibrate for ~1 week before the beginning of each experiment. During equilibration, the cores were kept in the dark, and the overlying water was

Acknowledgments

We thank Wei Wang for the construction of oxygen microelectrodes and assistance in the field. S. Seitzinger and G. Taghon helped improve early versions of the manuscript. We also thank B. Boudreau, B. Hales, and W. Martin for insightful reviews that helped refine this manuscript. This work was supported by the National Science Foundation (grant OCE-9496066).

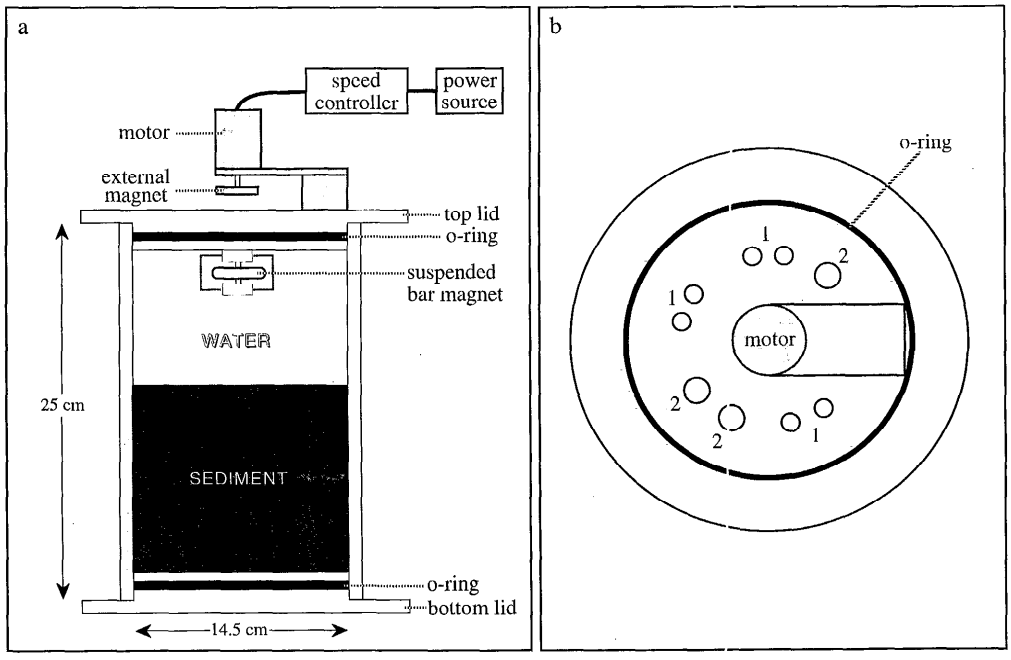

Fig 1. Side view (a) and top view (b) of flux chamber. The openings in the upper lid were used to accommodate pH, P_{CO_2}, and sulfide microelectrodes for sediment profiling or three-way stopcock valves for sample collection (1) and the reference electrode or pH, oxygen, and sulfide electrodes for monitoring the overlying water (2). Any openings that were not in use were tightly sealed with plastic plugs.

bubbled with air. No discernible color or topography changes were seen in the cores, and no macrofaunal activities were detected during this time.

Core incubation—The water overlying the sediment was stirred continuously without sediment resuspension. Stirring was accomplished by rotating a floating bar magnet at 100 rpm with an external motor (Fig. 1). Oxygen, pH, and sulfide electrodes were mounted through the chamber lid to allow continuous measurements in the overlying water (Fig. 1b).

Each core was incubated in the dark at ambient laboratory temperature (23–24°C) for ~40 h (Table 1). During incubation, overlying water samples were withdrawn from the chamber in a time series and analyzed for DIC. The volume removed by sampling was compensated for by adding stock seawater (collected from Schooner Creek at the time of sampling) through a second stopcock (Fig. 1b). At the end of incubation, additional samples were taken for chlorinity (to determine salinity), and large-volume samples (300 ml) were collected for DIC. These analytical procedures and their precisions (determined from replicate measurements of standards) are summarized in Table 2.

Microprofiling—Microelectrode profiles of pore-water pH and P_{CO_2} were measured directly before and after each incubation. Resistivity profiles were measured after each in-

Table 1. Microelectrode profiles and overlying-water analyses.

	Preincubation profiles*			Incubation		Postincubation profiles*		
Exp.	pH	P_{CO_2}	Other	Duration (h)	Analyses	pH	P_{CO_2}	Other
1	not reported†		—	36	DIC	1H-a′		
					pH‡	1H-b′	1C	Res
2	2H-a	2C-a	O_2	43	DIC	2H-a′	2C-a′	Res
	2H-b	2C-b	S^{2-}		pH‡	2H-b′	2C-b′	S^{2-}
					O_2‡	2H-c′		
					H_2S‡			
					chlorinity			

* pH and P_{CO_2} profile IDs as given in Fig. 4. The number represents Exp. 1 or Exp. 2; H and C represent pH and P_{CO_2}, respectively; postincubation profiles are primed. pH and P_{CO_2} profiles that were measured simultaneously are shown adjacent to each other. All other profiles (O_2, H_2S, Res [resistivity]) were measured after the pH and P_{CO_2} determinations.

† These profiles were not stable because the surface sediment was undergoing rapid chemical changes directly after ceasing the supply of O_2 to the chamber. However, they were similar to those of Exp. 2.

‡ Monitored in overlying water using electrodes.

Table 2. Chemical analyses applied to overlying-water, pore-water, and sediment samples.* NA = not available.

Analysis	Exp.	Method of detection	Sample size	Sample handling	Precision (±1 SD)	Reference
DIC	1 (olw, pw) 2 (olw)	Flow injection analysis	3 ml	Refrigerated in plastic syringes	<0.1 mmol kg^{-1}	Hall and Aller (1992)
DIC, salinity	1, 2 (olw)	SOMMA with coulometric detector and conductivity cell	300 ml	Poisoned with saturated $HgCl_2$	2 μmol kg^{-1} (DIC) 0.005‰ (salinity)	Johnson et al. (1993)
DIC	2 (pw)	Manometer†	1 ml	Filtered then frozen in crimped serum bottles	NA	Boehme et al. (1996)
Chlorinity	1 (olw, pw) 2 (olw)	Titration with $AgNO_3$, in 0.1-ml aliquots	5 ml (olw) 3 ml (pw)	Refrigerated in sealed glass vials	0.6‰	Grasshoff et al. (1983)
POC	1, 2	Combustion after acidification	<20 mg (dry wt)	Freeze-dried	0.06%	Hedges and Stern (1984)
δ^{13}C-POC	2	Modified Finnigan MAT Delta E isotope radio mass spectrometer†	<20 mg (dry wt)	Freeze-dried, acidified	NA	Hayes et al. (1977)

* olw, overlying water; POC, particulate organic carbon; pw, pore water, SOMMA, Single-Operator Multiparameter Metobolic Analyzer.
† Courtesy of Dr. N. Blair (North Carolina State Univ.).

cubation. O_2 and S^{2-} microprofiles were measured only during Exp. 2 (Table 1). Another difference between the two experiments was that in Exp. 1, the air supply to the overlying water was cut off at the beginning of the preincubation microelectrode measurements. This led to a rapid decline in oxygen concentration in the overlying water and to appreciable changes in chemical gradients of the pore water while the sediment was being profiled. Therefore, in Exp. 2, aeration was not terminated until the preincubation profiles were completed.

To profile the sediment, microelectrodes were inserted through 1-cm-diameter pluggable openings (Fig. 1b). They were lowered with a micromanipulator into the sediment at increments of 0.2 mm or larger until the tips were positioned at ~40 mm depth. The position of the sediment–water interface was determined visually with use of a magnifying glass. The sediment interface was designated as the position where the tip of the microelectrode met its shadow (created by illuminating the microelectrode from the side with a small lamp) with an estimated precision of ±0.1 mm. The pH and P_{CO_2} electrodes were mounted together (2.5 cm apart) and lowered simultaneously into the sediment. During preincubation conditions, up to 30 min was required at each depth within the upper 1 mm of the sediment for the P_{CO_2} sensor to record a steady signal. At all other depths and at each step of the postincubation profiles, 5–15 min was sufficient. Steady readings were obtained from oxygen, resistivity, sulfide, and pH electrodes in shorter amounts of time (<10 s for oxygen, 1–2 min for resistivity, and 1–10 min for sulfide and pH).

All profiles were measured at an equal radial distance (5.5 cm) from the center of the chamber. Also, because the stirring rate of the overlying water was kept constant, all profiled sites were assumed to have been exposed to a common hydrodynamic environment.

Electrode characteristics and calibration methods—pH: The pH microelectrodes used for sediment profiling were constructed as described by Cai and Reimers (1993) with tip diameters of ~200 μm (Fig. 2a). They were calibrated immediately after profiling in two buffer solutions made with synthetic seawater (DOE 1994). All measurements are reported in the total hydrogen ion scale. Calibration results are summarized in Table 3. During all measurements, the sensor signal was logged every 30 s by a digital data-logging system (Solus Systems). The outputs of P_{CO_2} and oxygen microelectrodes (*see below*) were also collected in the same manner.

Commercial pH electrodes were used to monitor the pH of the overlying water throughout both experiments. A combined pH–Ag/AgCl electrode (Cole Parmer), with a maximum drift of 2 mV over 2 d, was used in Exp. 1, and a combined pH–calomel electrode (Fisher Scientific) was used in Exp. 2. No stability tests were conducted for the pH–calomel electrode. These sensors were calibrated in the same manner as the microelectrodes.

P_{CO_2}: Potentiometric P_{CO_2} microelectrodes were constructed as described by Cai and Reimers (1993). However, a more rugged membrane at the sensor tip was prepared by letting a plug of silicone elastomer (Dow Corning MDX4-4210) cure within the outer glass capillary to a thickness of 50–100 μm (Fig. 2b). Small variations in membrane thickness did not appear to affect the response time of the electrode. The entire electrode body was filled with the electrolyte solution (1 mM $NaHCO_3$ and 0.7 M NaCl, saturated with AgCl), which eliminated the moisture buildup that can induce short-circuits. The P_{CO_2} microelectrodes exhibited near-Nernstian log-linear calibrations (Table 3) and little drift (<0.5 mV h^{-1}) and had a shelf life of several weeks.

The P_{CO_2} microelectrode used in Exp. 2 was calibrated in two steps. First, the calibration slope, or sensitivity, was determined immediately after each profiling session using a 0.7 M NaCl solution bubbled with known CO_2–N_2 gas mixtures, ranging from 0.36 matm (air) to 28.0 ± 0.1 matm. Subsequently, the electrode readings from each sediment profile were referenced to its readings in the overlying water, and the calibration slope and calculated P_{CO_2} values in the over-

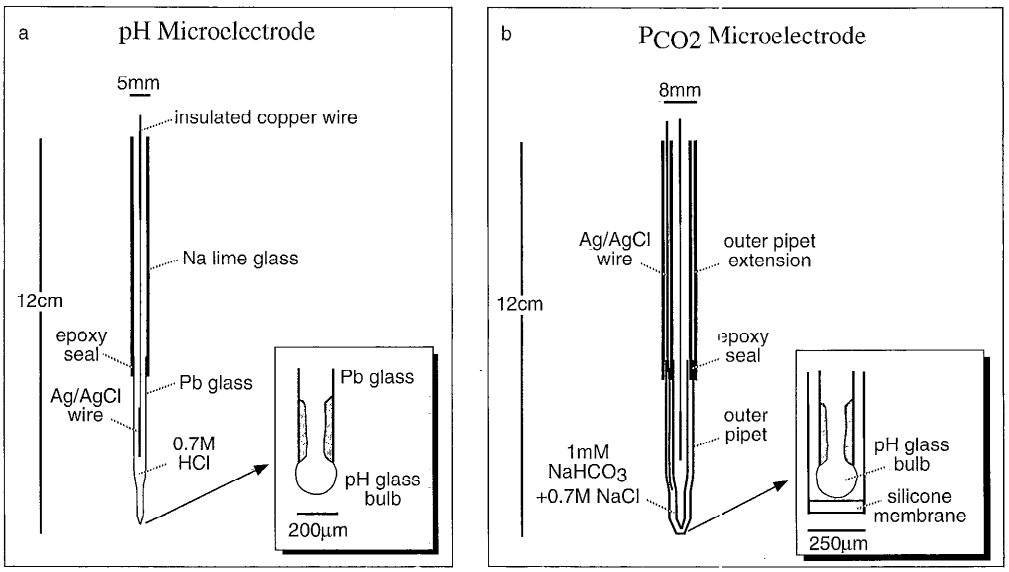

Fig. 2. Schematics of the pH (a) and P_{CO_2} (b) microelectrodes.

lying water were used to calculate P_{CO_2} values at each depth. The overlying water P_{CO_2} was calculated from pH values measured using the combined-pH electrode, measured DIC, and equilibrium relationships and constants from Weiss (1974) and Roy et al. (1993). Because the calibration gas mixtures did not bracket the highest P_{CO_2} values observed in the sediment, it was assumed that the electrode response remained log-linear over the entire P_{CO_2} range (theoretically, an electrode with 1 mM $NaHCO_3$ filling solution should show log-linear response between 0.66 and 260 matm [Jensen and Rechnitz 1979; Zhao and Cai 1997]).

In Exp. 1, the sensitivity determination for the P_{CO_2} microelectrode was confounded because the slope of the sensor calibration curve ($\Delta mV/\Delta \log P_{CO_2}$) was not Nernstian at low P_{CO_2} values. Therefore, a simplified three-point calibration was constructed using the electrode's output and P_{CO_2} values calculated from measured pH and DIC values in (1) overlying water, (2) pore water at a depth of 5 mm, and (3) pore water at a depth of 10 mm. It should be noted that this calibration method was not independent of the measured pore-water DIC, whereas the calibration approach applied in Exp. 2 was independent of the DIC measurements.

The P_{CO_2} microelectrodes also responded to changes in H_2S on an equimolar basis (calibration data not shown). The P_{CO_2} measurements from Exp. 2 were corrected for the effects of increasing H_2S concentrations using the sulfide microelectrode measurements. No corrections were applied to the P_{CO_2} determinations in Exp. 1 because this correction was inherent in the calibration constructed from pore-water P_{CO_2}.

Oxygen: A cathode-style oxygen microelectrode (Revsbech and Jørgensen 1986), with a tip size of ~10 µm, was used to measure preincubation O_2 profiles during Exp. 2. During tests before the profile measurements, it exhibited a rapid, linear response to increases in dissolved O_2 and negligible stirring effects. The profile was calibrated on the basis of a linear calibration defined by the electrode signal recorded in the anoxic part of the sediment and the overlying

Table 3. pH and P_{CO_2} electrode calibration results.

Exp.	Sensor	Incubation	Measured sensitivity at 23-24°C*	% theoretical
1	Combined pH	Pre	58.7	99.7
		Post	58.4	99.2
2	Combined pH	Pre	58.6	99.6
		Post	58.0	98.6
1	Microelectrode pH	Pre	59.1	100.4
		Post	58.4	99.2
2	Microelectrode pH†	Pre	59.0	100.4
		Post	58.6	99.6
1	P_{CO_2}	Post	56.1±0.3 (R^2=0.995, n=3)	95.2
2	P_{CO_2}	Pre	55.1±0.3 (R^2=0.997, n=4)	93.4
		Post	56.5±0.4 (R^2=0.999, n=3)	96.1

* Units are in $-(\Delta mV)/(\Delta pH$ unit) for pH and $(\Delta mV)/[\Delta \log(P_{CO_2})]$ for P_{CO_2}.

† Different reference electrodes, with different junction potentials, were inadvertently used for profiling and calibration procedures. Therefore, the microelectrode outputs were standardized against parallel pH measurements made with a commercial combined-pH electrode in the overlying water.

Table 4. Molecular diffusion coefficients of DIC species.

Exp.	Average temperature (°C)	Salinity (‰)	$D_{o,i}$ ($\times 10^{-5}$ cm^2 s^{-1}) H_2CO_3*	HCO_3^-	CO_3^{2-}	$D_{o,\Sigma}$ ($\times 10^{-5}$ cm^{2}s^{-1})
1	23.7±0.2 SD	26.7	1.71	1.08	0.875	1.27
2	23.1±0.2 SD	29.8	1.78	1.05	0.849	1.25

water, which was bubbled with air. Similarly, a Clark-style O_2 microsensor, with a built-in reference (Revsbech and Ward 1983), was used to monitor oxygen concentration in the overlying water in Exp. 2. Because this sensor was never inserted into the sediment, it was calibrated by assigning air-saturated O_2 concentrations to readings in air-bubbled overlying water and assuming that the sensor output during the anoxic period of the incubation was equal to a zero current (*see below*).

Sulfide: A potentiometric sulfide (S^{2-}) microelectrode (Revsbech and Jørgensen 1986) was used in Exp. 2 for sediment microprofiling and monitoring of overlying water. The diameter of the tip was ~100 μm. Calibrations, using a gas mixture of 1% H_2S in N_2 at different pH values, displayed a near-Nernstian response (within ±2%). Data were recorded by a pH meter and logged every 30 s during microprofiling and every 5 min during water monitoring. Microelectrode S^{2-} and pH values were used with the equilibrium constants of Millero (1995) and Smith and Martell (1976) for calculations of P_{H_2S} (partial pressure of H_2S).

Resistivity: Resistivity measurements were made in the sediment to determine the sediment formation factor (F). A resistivity sensor, similar to that of Andrews and Bennett (1981), was constructed with a wire spacing of 2 mm. Assuming that the sediment particles had negligible conductivity, resistivity recordings were converted to F using the following relationship:

$$F = \frac{R_S}{R_W}, \tag{1}$$

where R_S is the resistivity output at a specific depth in the sediment and R_W is the mean output of the sensor in the overlying water, which is assumed to be equal to the resistivity in the pore solution (McDuff and Ellis 1979; Andrews and Bennett 1981).

Pore-water and sedimentary organic carbon—The cores were extruded after the incubations and sectioned at 2.5-mm intervals to 10 mm and at 5-mm intervals to 40 mm. Pore water was extracted by centrifugation (5,000 rpm for 10 min), filtered (0.45 μm), and analyzed for DIC and chlorinity (to determine salinity, Exp. 1 only). Particulate organic and inorganic carbon content (in weight percent [wt%] of dry sediment) and the $\delta^{13}C$ value of sedimentary carbon (Exp. 2 only) were also determined (Table 2).

Diffusive fluxes of DIC—Diffusive fluxes of DIC were obtained through two methods. In the first method, $J_{\text{DIFF-L}}$ was determined as follows:

$$J_{\text{DIFF-L}} = -\frac{1}{F_{\text{avg}}} \sum D_{0,i} \frac{dC_i}{dz}, \tag{2}$$

where

C_i = concentration (per unit volume of pore water) of each of the DIC species i: CO_3^{2-}, HCO_3^-, and $H_2CO_3^*$ (total undissociated CO_2), calculated from the pH and P_{CO_2} profiles;

z = depth in sediment below the sediment–water interface (positive downward);

dC_i/dz = gradient of species i within the upper millimeter of sediment calculated from linear regression on determinations within this zone;

$D_{0,i}$ = molecular diffusion coefficient of species i corrected for temperature and salinity (calculated from Himmelblau 1964; Broecker and Peng 1974; Li and Gregory 1974; *see Table 4*); and

F_{avg} = average formation factor within the upper millimeter of sediment.

Eq. 2 is derived from Fick's First Law,

$$J_{\text{DIFF-L}} = -\phi \sum D_{S,i} \frac{dC_i}{dz}, \tag{3}$$

as well as the following empirical relations:

$$D_{S,i} = \frac{D_0}{\theta^2} \tag{4}$$

and

$$\theta^2 = \phi F, \tag{5}$$

where ϕ is the porosity, $D_{S,i}$ is the whole-sediment diffusion coefficient of species i, and θ is the sediment tortuosity (Berner 1980; Ullman and Aller 1982).

In the second method, $J_{\text{DIFF-C}}$ was calculated after finding the best fit of an exponential curve,

$$C_z = A \exp(-Bz) + D, \tag{6}$$

for each DIC profile (0–40 mm) using a least-squares analysis. In Eq. 6, A, B, and D are fitting parameters. The diffusive fluxes were then calculated as follows:

$$J_{\text{DIFF-C}} = -\frac{1}{F_{\text{avg}}} \sum D_{0,\Sigma} \left.\frac{dC_z}{dz}\right|_{z=0}, \tag{7}$$

where $D_{0,\Sigma}$ is a weighted diffusion coefficient for DIC determined from the concentration ratios and the molecular diffusion coefficients of $H_2CO_3^*$ and HCO_3^-, and $dC_z/dz|_{z=0}$ is the derivative of Eq. 6 evaluated at $z = 0$.

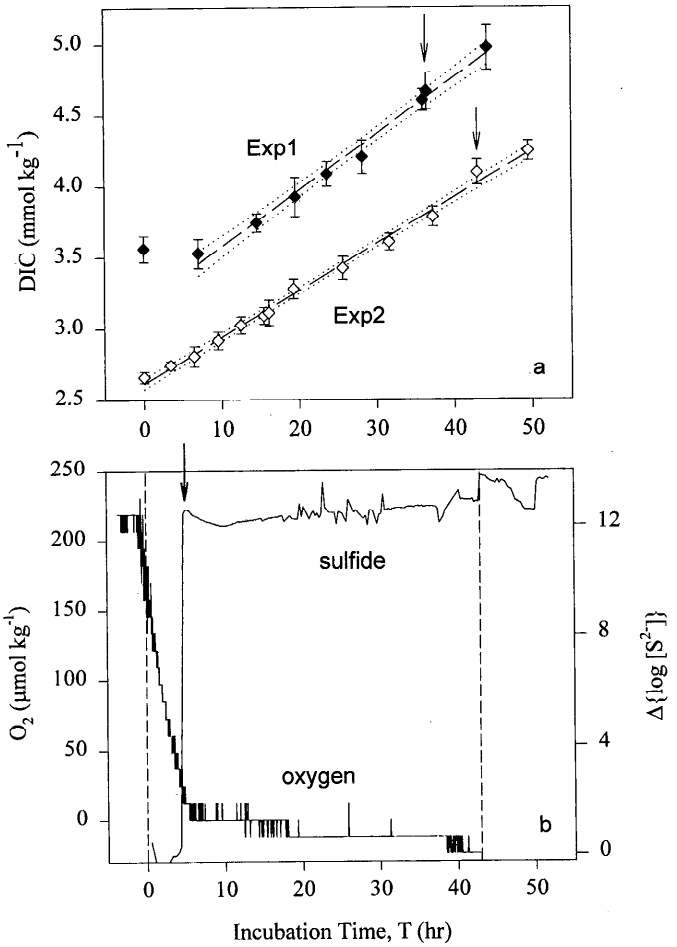

Fig. 3. Overlying-water time series of DIC (a) and oxygen and sulfide monitored using microelectrodes in Exp. 2 (b). In a, arrows indicate the end of the incubation periods. Microelectrode profiles were measured during ~10 h periods before each incubation and during the time interval bracketed by the last two DIC samples. DIC concentrations were corrected for dilution caused by volume compensation during the sampling process. Error bars are ±1 SD, and dotted lines indicate 95% confidence limits of the regression curves. The data point at $T = 0$ h in Exp. 1 was excluded from the regression because after this time point, >70 ml of overlying water had to be added to the chamber to compensate for the volume drawn out for various samples. In b, the sulfide electrode reading is reported as the change in log[S^{2-}] with respect to the preincubation conditions. The two dashed lines bracket the incubation period, and the arrow denotes the suspected time of anoxia in the water column.

Results

Time-series measurements in overlying water—Total flux of DIC: During the periods of closed incubation, DIC concentrations in the overlying water increased linearly with time in both experiments (Fig. 3a). Total fluxes, J_{TOT}, were calculated by dividing the slope of the linear regressions portrayed in Fig. 3a by the sediment surface area, then multiplying these quotients by the volume and density of the overlying water. Errors were estimated from the standard errors of the regression coefficients after appropriate unit conversions. The total fluxes were 4.4 ± 0.2 and 3.5 ± 0.1 mmol m^{-2} h^{-1} for Exp. 1 and Exp. 2, respectively, and these values were significantly different ($P = 0.05$) from each other.

Oxygen and sulfide: During Exp. 1, the overlying water was already depleted in oxygen at the start of the incubation period (*see Materials and methods*). During Exp. 2, however, oxygen concentration decreased rapidly from $T = 0$ until $T = 5$ h when a shift in redox equilibria was observed (Fig. 3b). The small decrease in the oxygen sensor signal after this time was likely caused by either hysteresis or sulfide poisoning, and it was assumed that the chamber became anoxic 5 h after the beginning of the incubation. The observation that a discernible break did not occur in the DIC time course at the estimated time of anoxia of Exp. 2 (Fig. 3a) suggests a minor role of oxic respiration in determining the inorganic carbon production rates of these sediments.

Sediment profiles—A total of seven pH profiles and five P_{CO_2} profiles are reported from the two experiments (Table 1). The differences between the pre- and postincubation microelectrode profiles of pH, P_{CO_2}, and sulfide in Exp. 2 (Fig. 4) show that the pore-water chemistry near the sediment surface was appreciably different before and after this incubation. The Exp. 1 pre- and postincubation profiles also showed this change. However, the preincubation profiles (attempted immediately after ceasing the supply of oxygen to the overlying water) are not reported because they were changing too rapidly to record accurately.

pH: Preincubation pH profiles from Exp. 2 decreased by as much as 2.5 pH units within the first few millimeters of sediment and exhibited a high degree of near-surface spatial heterogeneity (Fig. 4c). On the other hand, postincubation profiles had a maximum change of only 0.15 pH units and less spatial heterogeneity (Fig. 4a,c). The overlying water pH values decreased by ~1.5 units during the incubation, but pore-water values at 40 mm depth appeared relatively unchanged throughout both experiments (Fig. 4c).

A precision of better than ±0.02 pH units was estimated from the standard deviations of four or more sensor readings recorded at each depth. A larger standard deviation of ±0.03 pH units was assigned for the Exp. 2 postincubation profiles to account for an external source of electrical noise that persisted during these measurements.

Oxygen and sulfide: Preincubation O_2 and S^{2-} microprofiles from Exp. 2 indicate a sharp redox boundary close to the sediment–water interface and rapid oxygen uptake by the sediment (Fig. 4e,f). The preincubation P_{H_2S} profile was calculated from S^{2-} and pH values that were averages of the two preincubation pH profiles. Because pH was extremely low near the interface during preincubation conditions, a greater portion of the total sulfide was H_2S, so P_{H_2S} appears elevated. After the incubation, the overlying water P_{H_2S} had increased to ~0.25 matm, and P_{H_2S} increased steadily with depth in the sediment to ~25 matm at 40 mm.

P_{CO_2}: The overlying-water P_{CO_2} values increased during

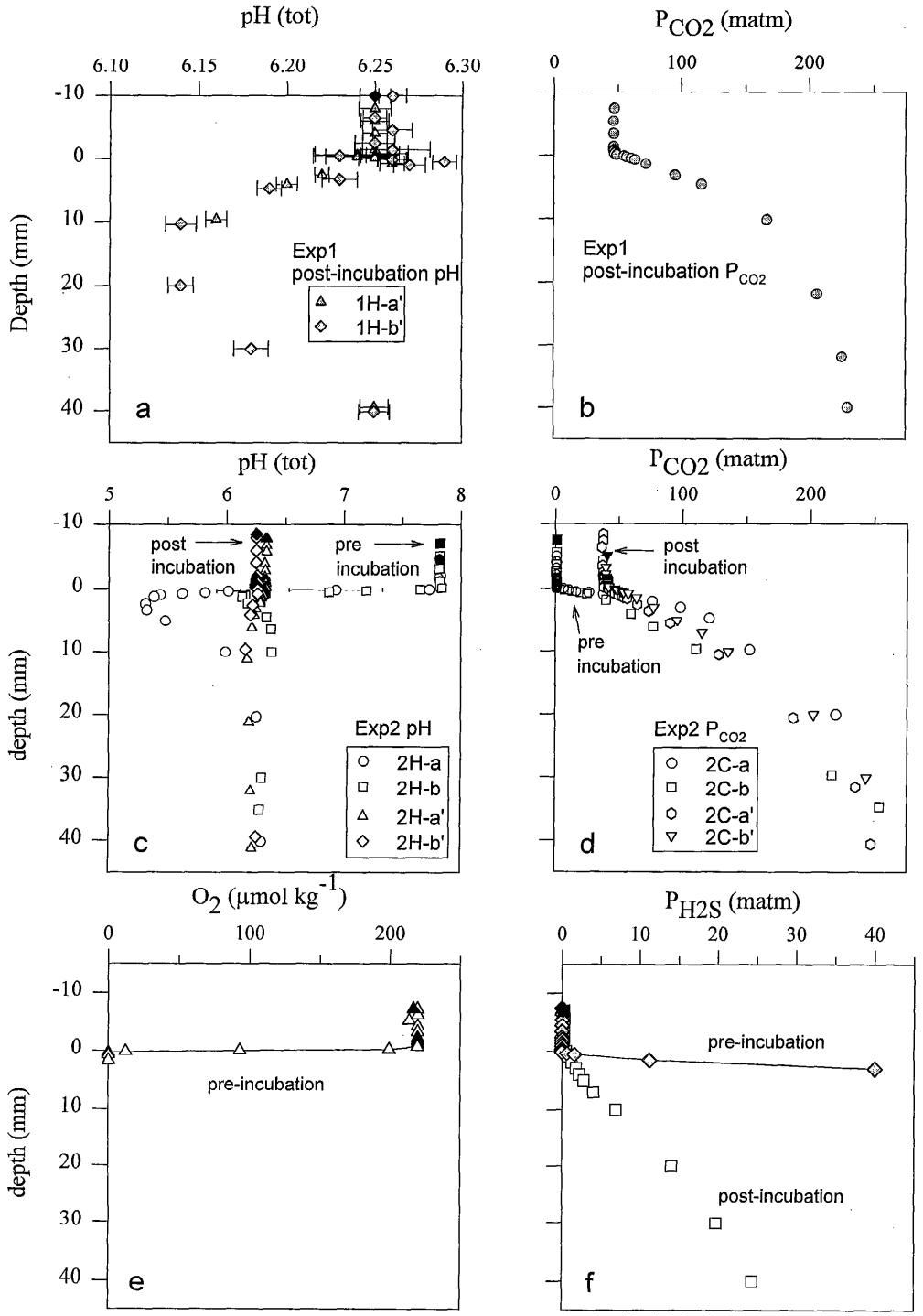

Fig. 4. Microelectrode profiles of pH (a, c), P_{CO_2} (b, d), O_2 (c), and H_2S (f). Error bars represent ±1 SD. In all figures, filled symbols represent readings taken after the sensor was retracted from the sediment.

Exp. 2 from ~0.85 to 40 matm (Fig. 4d). P_{H_2S} accounted for less than 1% of the P_{CO_2} sensor signal within the upper 1 mm of the sediment and reduced the P_{CO_2} gradient by <4% in that depth zone. By 40 mm, P_{H_2S} amounted to ~10% of the P_{CO_2} microelectrode signal.

One postincubation P_{CO_2} profile (2C-b′) was measured at an intact spot, whereas another (profile 2C-a′) was measured along the rim of a cavity created during the preincubation profile. Near the cavity, the tip of the electrode approached the sediment surface at an angle; therefore, data points in

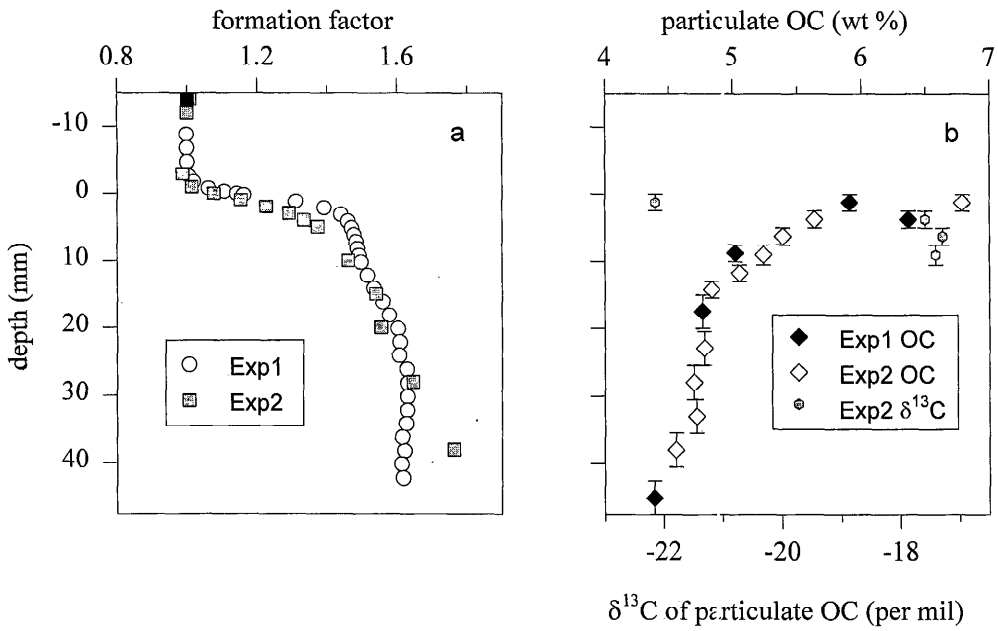

Fig. 5. Formation factor profiles (a) and particulate organic carbon and $\delta^{13}C$ values within the upper 10 mm of the sediment column (b). Formation factors were determined from resistivity data according to Eq. 1. The filled symbol represents the reading taken after the resistivity sensor was retracted from the sediment. The vertical error bars in b represent the depth interval of the sample.

the uppermost few millimeters of profile 2C-a′ probably underestimate the average P_{CO_2} gradient.

The precision of the P_{CO_2} microelectrode measurements was estimated in the same manner as for pH. Generally, all points have uncertainties of ±3% (coefficient of variation [CV]) or better.

Formation factor: Formation factor increased sharply at the sediment–water interface and approached values of 1.6 or greater by 20 mm depth (Fig. 5a). The relationship between F and porosity, $F = \phi^{-m}$, where m is an empirically determined constant (Ullman and Aller 1982), was investigated by making independent F and ϕ measurements on slurries prepared from Schooner Creek sediment. Using the determined m values (2.4 and 2.8 for Exp. 1 and Exp. 2, respectively) in the above relationship, formation factor profiles were converted to porosity profiles. The predicted porosity profiles agreed well with porosity measurements made independently by weight loss after the cores were sectioned (data not shown), validating the resistivity measurements.

Particulate carbon: The organic carbon content of both cores varied from 6 to 7 wt% near the sediment surface to ~4.5 wt% near 40 mm (Fig. 5b). The inorganic carbon content was negligible (<0.25 wt%) in both cores at all depths. Isotopic values of particulate organic carbon determined in the upper 2–8 mm of sediment were near −17‰ uniformly (Fig. 5b). We believe this value reflects the mixed inputs of marine detritus and *Spartina alterniflora,* the dominant surface vegetation in Schooner Creek (Szedlmayer and Able 1993). In contrast, the measured isotopic value of the organic carbon from 0 to 2 mm was approximately −22‰. We suspect this unique character resulted from the presence of the microbial mat.

DIC profiles—Pore-water DIC profiles were calculated from pH and P_{CO_2} microelectrode data using CO_2 gas solubility and carbonic acid dissociation constants based on the total hydrogen ion scale at the appropriate temperatures and salinities (Weiss 1974; Roy et al. 1993). Two DIC profiles were determined from the Exp. 1 postincubation measurements (Table 5, Fig. 6a). Two DIC profiles were calculated from the Exp. 2 preincubation measurements (not shown), and four DIC profiles were calculated from the Exp. 2 postincubation measurements (Table 5, Fig. 6b). Ideally, to eliminate errors caused by spatial heterogeneity, each point of a DIC profile should be calculated from pH and P_{CO_2} values determined at a common point. In this study, the pH and P_{CO_2} electrodes were separated by 2.5 cm or more. The good reproducibility of the pH and P_{CO_2} profiles during postincubation conditions (Fig. 4a,c,d), however, justifies pairing these measurements to determine DIC profiles. The precision of the calculated DIC values (±4 to ±7% CV) was derived by propagating the standard deviations of pH and P_{CO_2} measurements (Miller and Miller 1984).

All microelectrode DIC profiles increased to 20–25 mmol kg^{-1} at 40 mm depth (Fig. 6). In Exp. 2, the microelectrode DIC values from postincubation conditions overlapped in some cases with the independent data obtained by pore-water extraction, but, on average, the microelectrodes gave lower values (Fig. 6d).

Microelectrode DIC profiles calculated from the preincubation measurements of Exp. 2 are not shown or included in the following calculations because they each have one or

Table 5. Calculated and measured fluxes of DIC.*

	Microelectrode measurements					Pore-water extraction		Total flux
	Profiles			J_{DIFF} (mmol m^{-2} h^{-1})		J_{DIFF} (mmol m^{-2} h^{-1})		J_{TOT} (mmol m^{-2} h^{-1})
Exp.	DIC	pH	P_{CO_2}	J_{DIFF-L}	J_{DIFF-C}	J_{DIFF-L}	J_{DIFF-C}	
1	M1	1H-a′	1C	5.8±0.5	4.9±0.6	6.4	5.1±0.6	4.4±0.2
	M2	1H-b′	1C	6±2	5.0±0.5			
			Combined†	5.9±1	4.9±0.4			
2	$J3_{adj}$‡	2H-a′	2C-a′		3.0±0.5	9.4	5.7±0.6	3.5±0.1
	$J4_{adj}$	2H-b′	2C-b′	5.1±0.8	4.7±0.3			
	J5§	2H-c′	2C-a′		4.0±0.4			
	J6§	2H-c′	2C-b′		3.9±0.4			
			Combined†		4.0±0.4			

* Errors represent ±1SE.

† Combined values were determined by pooling all data points from all the individual profiles into one model profile and applying the same calculation procedures.

‡ Surface gradient was not calculated from this profile because of uncertainty in the uppermost portion of profile 2C-a′ (*see text*). The subscript adj indicates that the pH and P_{CO_2} profiles were measured as a pair (2.5 cm apart).

§ Surface gradients were not calculated for these profiles because of the lack of pH data points near the sediment–water interface.

two points that appear as a large subsurface maximum (~14 mmol kg^{-1}). We consider this an artifact because it requires a zone of intense DIC production that is two orders of magnitude higher than J_{TOT}. These DIC peaks may have resulted from mismatching of the acute and spatially heterogeneous pH and P_{CO_2} gradients that existed during preincubation conditions (Cai and Reimers 1993), or the carbonate system may not have attained thermodynamic equilibrium within the surface sediment because of very rapid CO_2 production (de Beer et al. 1997; *see Discussion*).

Diffusive flux of DIC—J_{DIFF-L}: Values of J_{DIFF-L} were calculated using Eq. 2 and microelectrode measurements from within the upper 1 mm of sediment (Table 5, Fig. 6c) as equal to 5.8 ± 0.3 and 6 ± 2 mmol m^{-2} h^{-1} in Exp. 1 and 5.1 ± 0.8 mmol m^{-2} h^{-1} in Exp. 2 (Table 5). The formation factor (F) in the first millimeter of sediment was assumed to equal 1.20 and 1.11 in Exp. 1 and 2, respectively (*see also Fig. 5*). Errors were estimated from the largest of the three standard errors of regression (i.e., the regressions through the gradients of the three DIC species) after appropriate unit conversions. Because the number of data points used to calculate the gradients of the DIC species was small, the errors associated with the estimates of these slopes and thus J_{DIFFL} were large compared with other flux estimates (Table 5). In all cases, the flux of CO_3^{2-} was negligible, and the HCO_3^- flux ranged from 56 to 65% of the total flux. Although these values of J_{DIFF-L} are all consistently greater than the corresponding values of J_{TOT}, the differences are not significant (P = 0.05, mean ± 2 SE).

J_{DIFF-C}: Examples of the exponential curve fits (Eq. 6) that were used to calculate values of J_{DIFF-C} according to Eq. 7 are shown in Fig. 6. From the microelectrode data, the weighted diffusion coefficients for DIC, $D_{0,\Sigma}$, were evaluated to be 1.27 and 1.25 cm^2 s^{-1} for Exp. 1 and Exp. 2, respectively (Table 4). Errors were estimated by varying the value of B in Eq. 6 by ±1 SE, because J_{DIFF-C} was most sensitive to this parameter. J_{DIFF-C} values thus calculated were consistently lower than J_{DIFF-L} values because the exponential curves slightly underestimated the surface DIC gradient (Fig. 6c). However, overall, J_{TOT}, J_{DIFF-L}, and J_{DIFF-C} were not significantly different from each other (P = 0.05, mean ± 2 SE) (Table 5).

Pore-water extraction data: J_{DIFF-L} and J_{DIFF-C} were also calculated using the data from pore-water extraction (Table 5). To calculate J_{DIFF-L}, we applied a formula analogous to Eq. 7, using the DIC gradient measured between the uppermost datum and the overlying water (Fig. 6c,d). Values of $D_{0,\Sigma}$ were equal to those used to calculate J_{DIFF-L} (Table 4). The resulting J_{DIFF-L} was 6.4 mmol m^{-2} h^{-1} in Exp. 1, in reasonable agreement with J_{TOT}. In Exp. 2, however, it was 9.4 mmol m^{-2} h^{-1}, exceeding J_{TOT} by 170%. Similarly, J_{DIFF-C} obtained from a curve fit to the pore-water extraction data agreed within limits with J_{TOT} in Exp. 1 but exceeded J_{TOT} by 63% in Exp. 2. These results are not surprising considering the weighted importance of the DIC concentration determined for the first, relatively coarse depth interval in the extracted pore-water profile (Fig. 6c).

Discussion

To begin a discussion of our experiments, we first verify that the conditions outlined as necessary for the total flux of DIC (J_{TOT}) to equal the diffusive flux (J_{DIFF}) were met. These conditions were that (1) the rate of DIC production must be time-independent (i.e., zero-order) and (2) the diffusion of DIC across the sediment–water interface must be the dominant process adding DIC to the overlying water.

The zero-order condition is supported by the linear increase of DIC in the overlying water with time, both during and after the incubations (Fig. 3a). This suggests that the DIC gradient near the sediment–water interface was constant with time and that the J_{DIFF} value determined at the end of the incubation represents the entire experiment. Two processes must be considered to evaluate the second condition: (1) bioirrigation and (2) flux of methane to the overlying water followed by oxidation to CO_2. Both processes should cause J_{DIFF} to be smaller than J_{TOT}. We know the effect of

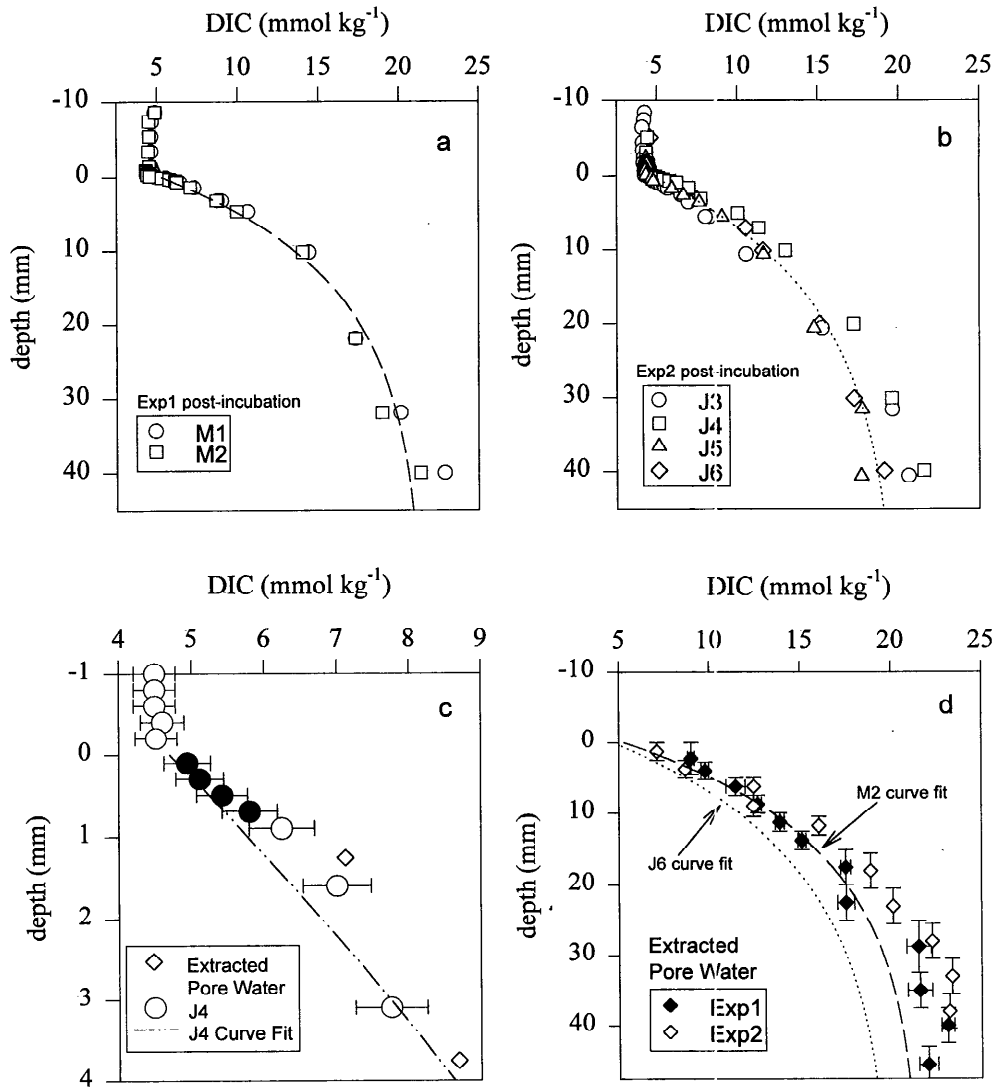

Fig. 6. DIC profiles calculated from microelectrode measurements (a–c) (*see Table 5* for profile IDs) and measured by pore-water extraction (d). In a and b, the dashed and dotted lines are best-fit curves for profiles M2 and J6, respectively, as calculated from Eq. 6. In c, an example of a microelectrode-derived near-surface DIC gradient is illustrated. The diffusive DIC flux corresponding to this profile was calculated using the pH and P_{CO_2} data that predict the filled circles. Similar surface gradients were obtained from the remaining DIC profiles. Measured pore-water DIC values for Exp. 2 are also plotted for comparison. Horizontal error bars represent ±1 SD. In d, pore-water extraction results are plotted, along with best-fit curves for M2 and J6 for comparison. Vertical error bars represent the depth interval of the sample. Horizontal error bars represent ±1 SD.

bioirrigation was minimal, because the observed number of macrofauna was low and their activities stopped under the low levels of oxygen in the chamber during the incubations (Rutgers van der Loeff et al. 1984). We also measured $\delta^{13}C$ values of overlying- and pore-water DIC during Exp. 2. These data and mass-balance calculations suggest that methane oxidation had a negligible impact on the flux of DIC (Komada 1996).

The conditions required to equate J_{TOT} with J_{DIFF} were thus met in both experiments. The findings that J_{TOT} and microelectrode-derived values of J_{DIFF} agreed within 50% and were not significantly different from each other ($P = 0.05$) can therefore be interpreted as corroboration that paired pH and P_{CO_2} measurements can be used to derive valid DIC gradients and diffusive fluxes. Below, we discuss other conclusions that can be drawn from our data and calculations.

How typical were these sediments?—The oxygen, sulfide, and pH microprofiles measured at the beginning of Exp. 2 were similar to other profiles measured across the sediment–water interface of anoxic sediments with microbial mats (Jørgensen and Revsbech 1983; Jørgensen and Des Marais 1990). The only exception was that the pH minimum was extremely low in the preincubation profiles, suggesting very

high rates of sulfide oxidation. The DIC production rates measured over the incubation were also high but not atypical of CO_2 fluxes from wetlands at temperatures >20°C (Raich and Potter 1995).

Diffusive flux calculations—There are three major assumptions made in the determination of J_{DIFF} using DIC gradients and Eqs. 2 and 7. First, surface roughness is negligible, so diffusion gradients are only one-dimensional in the vertical. Second, microelectrodes have no impact on the chemical gradients they measure. Third, diffusion through microbial mats is analogous to diffusion through bulk sediment. The potential effect of microbial mat microtopography on calculated diffusive fluxes has been investigated by Jørgensen and Des Marais (1990). They found that the surface area of a mat, and consequently the upper boundary of its overlying diffusive boundary layer, may be larger than a flat plane by 31 and 14%, respectively. These effects were shown to lead to a 49% underestimation when O_2 fluxes were calculated by Fick's First Law using microelectrode gradients measured perpendicular to the horizontal plane and across the diffusive boundary layer. A similar study was conducted by Gundersen and Jørgensen (1990) using a sandy mud collected along the coast of Denmark. They concluded that the oxygen diffusional flux may be underestimated by a factor of 2.5 because of the effects of microtopography.

No microscopic surface area measurements were made in this study, therefore, the extent of this effect on the calculated DIC flux is unknown. A diffusive oxygen flux calculated from the oxygen gradient measured within the diffusive boundary layer in Exp. 2 (Fig. 4e) is 4.2 mmol m^{-2} h^{-1}, compared with a total oxygen flux of 5.6 mmol m^{-2} h^{-1} determined from the initial rate of decrease in oxygen concentration in the overlying water (from $T = 0$ to $T = 1$ h, Fig. 3b). These calculations are consistent with a surface-area effect that tends to cause diffusive fluxes to be underestimated. However, because our DIC diffusive fluxes were calculated from gradients in the sediment rather than gradients in the diffusive boundary layer, the topographic influence may be less important than has been observed for O_2.

Another complication associated with the determination of J_{DIFF} may arise from microelectrode effects on interfacial gradients. Glud et al. (1994*b*) have shown that a microsensor approaching the surface of a sediment compresses the diffusive boundary layer, which can lead to a steepening of the diffusive boundary layer gradient and overestimation of the diffusive flux. This effect may also heighten gradients in the first millimeter of the sediment and explain our consistently greater estimates of $J_{DIFF\text{-}L}$ compared with J_{TOT}. Further laboratory studies with pH and P_{CO_2} sensors are required to investigate this effect.

Lastly, the assumption that the empirically derived analogy between porosity and molecular diffusivity, as described by Eqs. 1, 4, and 5, holds at the interface of sediments covered with a microbial mat is interesting to consider. Revsbech (1989) and Glud et al. (1995) studied the diffusivity of microbial communities by measuring the microgradients of O_2 and N_2O across a biofilm/microbial mat and the overlying diffusive boundary layer using microsensors. In both studies, investigators found that the conventional tortuosity–diffusivity relationships cannot be used for such microbial communities and attributed this observation to either a unique diffusional environment created by the high content of extracellular polymers with microbial films or mats or the presence of isolated cellular fluids that prevent accurate measurement of effective porosity (and hence the sediment diffusion coefficient). Using the empirical relationship $D_S = D_0\phi^{8.5}$, which Glud et al. (1995) proposed as a means to account for diffusivity within a mat, J_{DIFF} values may be reduced by 66 and 33% in Exp. 1 and 2, respectively.

CO_2 system disequilibria—Determination of DIC from P_{CO_2} and pH measurements assumes the CO_2 system to be at equilibrium. Metabolic CO_2 produced in the sediment follows two paths to reach equilibrium with the surrounding medium (1) hydration of $CO_{2(aq)}$ to form H_2CO_3, followed by (2) dissociation of H_2CO_3 to produce H^+, HCO_3^-, and CO_3^{2-}. Compared with the rapid acid-base reactions in step 2, the rate of step 1 is slow and limits the rate of the overall process (Stumm and Morgan 1981). The characteristic hydration time of $CO_{2(aq)}$ (or the time required for $CO_{2(aq)}$ to reach $1/e$ of its initial concentration) at 25°C is on the order of 30 s. Therefore, at least several minutes are required for the CO_2 system to reach equilibrium with its surroundings (Stumm and Morgan 1981).

Throughout our calculations, DIC was determined from pH and P_{CO_2} assuming the CO_2 system to be at equilibrium. However, near the sediment–water interface, where CO_2 production was most rapid in these experiments, equilibrium may not have been achieved because of the finite rate of $CO_{2(aq)}$ hydration and differential diffusion of carbonate species (de Beer et al. 1997). In such a case, DIC can be overestimated, especially in the pH range where HCO_3^- is favored over $CO_{2(aq)}$ and H_2CO_3 (above pH = 6.3 $\approx pK_1$). During preincubation conditions, pH dropped sharply within the upper 1 mm of the sediment column from near 7.7 to below 6.3 (Fig. 4c). This probably contributed to the apparent DIC peaks immediately below the sediment surface (*see Results,* DIC profiles). We are unable to establish with complete certainty whether equilibrium was achieved during postincubation conditions. It must be pointed out, however, that pH was near pK_1 and varied by only 0.03 units or less within the upper 1 mm of sediment (Fig. 4c). Therefore, had the CO_2 system not reached equilibrium, the degree of DIC overestimation would probably have been similar for all data points used to determine the DIC gradient, and, consequently, the effect on the magnitude of J_{DIFF} would be minimal.

Application to deep-sea sediments—DIC gradients, and hence pH and P_{CO_2} gradients, can be much smaller or almost nonexistent in deep-sea sediments (Hales et al. 1994; Hales and Emerson 1996, 1997; Hulth et al. 1997). Therefore, a final issue worth exploring is whether deep-sea DIC fluxes can be estimated accurately from in situ pH and P_{CO_2} microelectrode measurements. Three positive factors are that pH and P_{CO_2} profiles in such environments may be described adequately with coarser vertical resolution, CO_2 disequilibria is unlikely to be an issue, and total deep-sea fluxes are likely to be dominated by diffusion. However, the deep-sea challenge is that much higher precision and accuracy in the pH

and P_{CO_2} measurements are required. The uncertainty in our current DIC estimates was as large as 7%. What can be achieved in situ should be a few percent better because laboratory pH and P_{CO_2} measurements are unavoidably noisier than in situ readings (Hales and Emerson 1996). A larger number of profiles with less spacing between the pH and P_{CO_2} electrodes is also a means to reduce the uncertainty of this approach when defining DIC gradients. As P_{CO_2} sensors become easier to fabricate and more reliable in the field (Hales and Emerson 1997; Zhao and Cai 1997), we believe this approach will provide accurate deep-sea DIC fluxes.

References

ANDREWS, D., AND A. BENNETT. 1981. Measurements of diffusivity near the sediment–water interface with a fine-scale resistivity probe. Geochim. Cosmochim. Acta **45:** 2169–2175.

ARCHER, D., AND A. DEVOL. 1992. Benthic oxygen fluxes on the Washington shelf and slope: A comparison of in situ microelectrode and chamber flux measurements. Limnol. Oceanogr. **37:** 614–629.

———, S. EMERSON, AND C. REIMERS. 1989. Dissolution of calcite in deep-sea sediments: pH and O_2 microelectrode results. Geochim. Cosmochim. Acta **53:** 2831–2845.

BERELSON, W. M., D. E. HAMMOND, AND K. S. JOHNSON. 1987. Benthic fluxes and the cycling of biogenic silica and carbon in two southern California borderland basins. Geochim. Cosmochim. Acta **51:** 1345–1363.

———, ———, D. O'NEILL, X.-M. XU, C. CHIN, AND J. ZUKIN. 1990. Benthic fluxes and pore-water studies from sediments of the central north Pacific: Nutrient diagenesis. Geochim. Cosmochim. Acta **54:** 3001–3012.

BERNER, R. A. 1980. Early diagenesis: A theoretical approach. Princeton Univ. Press.

BOEHME, S. E., N. E. BLAIR, J. P. CHANTON, AND C. S. MARTENS. 1996. A mass balance of ^{13}C and ^{12}C in an organic-rich methane-producing marine sediment. Geochim. Cosmochim. Acta **60:** 3835–3848.

BROECKER, W. S., AND T.-H. PENG. 1974. Gas exchange rates between air and sea. Tellus **26:** 21–35.

BURDIGE, D. J., AND J. HOMSTEAD. 1994. Fluxes of dissolved organic carbon from Chesapeake Bay sediments. Geochim. Cosmochim. Acta **58:** 3407–3424.

CAI, W.-J, AND C. E. REIMERS. 1993. The development of pH and pCO_2 microelectrodes for studying the carbonate chemistry of pore-waters near the sediment–water interface. Limnol. Oceanogr. **38:** 1762–1773.

———, ———, AND T. SHAW. 1995. Microelectrode studies of organic carbon degradation and calcite dissolution at a California continental rise site. Geochim. Cosmochim. Acta **59:** 497–511.

DE BEER, D., A. GLUD, E. EPPING, AND M. KÜHL. 1997. A fast-responding CO_2 microelectrode for profiling sediments, microbial mats, and biofilms. Limnol. Oceanogr. **42:** 1590–1600.

DOE 1994. Handbook of methods for the analysis of the various parameters of the carbon dioxide system in seawater, version 2, A.G. Dickson and C. Goyet, eds. ORNL/CDIAC-74. U.S. Department of Energy. Unpublished manuscript.

GLUD, R. N., J. K. GUNDERSEN, B. B. JØRGENSEN, N. P. REVSBECH, AND H. D. SCHULZ. 1994*a*. Diffusive and total oxygen uptake of deep-sea sediments in the eastern South Atlantic Ocean: *In situ* and laboratory measurements. Deep-Sea Res. **41:** 1767–1788.

———, ———, N. P. REVSBECH, AND B. B. JØRGENSEN. 1994*b*. Effects on the benthic diffusive boundary layer imposed by microelectrodes. Limnol. Oceanogr. **39**: 462–467.

———, K. JENSEN, AND N. P. REVSBECH. 1995. Diffusivity in surficial sediments and benthic mats determined by use of a combined N_2O–O_2 microsensor. Geochim. Cosmochim. Acta **59:** 231–237.

GRASSHOFF, K., M. EHRHARDT, AND K. KREMLING. 1983. Methods of seawater analysis, 2nd ed. Verlag Chemie.

GUNDERSEN, J. K., AND B. B. JØRGENSEN. 1990. Microstructure of diffusive boundary layers and the oxygen uptake of the sea floor. Nature **345:** 604–607.

HALES, B., AND S. EMERSON. 1996. Calcite dissolution in sediments of the Ontong-Java plateau: In situ measurements of pore water O_2 and pH. Global Biogeochem. Cycles **10:** 527–541.

———, AND ———. 1997. Calcite dissolution in sediments of the Ceara rise: In situ measurements of pore water O_2, pH, and $CO_{2(aq)}$. Geochim. Cosmochim. Acta **61:** 501–514.

———, ———, AND D. ARCHER. 1994. Respiration and dissolution in the sediments of the western North Atlantic: Estimates from models of in situ microelectrode measurements of porewater oxygen and pH. Deep-Sea Res. **41:** 695–719.

HALL, P. O. J., AND R. C. ALLER. 1992. Rapid, small-volume, flow injection analysis for ΣCO_2 and NH_4^+ in marine and freshwaters. Limnol. Oceanogr. **37:** 1113–1119.

HAYES, J. M., D. J. DES MARAIS, D. W. PETERSON, D. A. SCHOELLER, AND S. P. TAYLOR. 1977. High precision stable isotope ratios from microgram samples. Adv. Mass Spectrom. **7:** 475–480.

HEDGES, J. I., AND J. H. STERN. 1984. Carbon and nitrogen determinations of carbonate-containing solids. Limnol. Oceanogr. **29:** 657–663.

HIMMELBLAU, D. M. 1964. Diffusion of dissolved gases in liquids. Chem. Rev. **64:** 527–550.

HULTH, S., A. TENBERG, A. LANDÉN, AND P. O. J. HALL. 1997. Mineralization and burial of organic carbon in sediments of the southern Weddell Sea (Antarctica). Deep-Sea Res. **44:** 955–981.

JENSEN, M. A., AND G. A. RECHNITZ. 1979. Response time characteristics of the pCO_2 electrode. Anal. Chem. **51:** 1972–1977.

JOHNSON, K. M., K. D. WILLS, D. B. BUTLER, W. K. JOHNSON, AND C. S. WONG. 1993. The performance of an automated continuous gas extractor and coulometric detector. Mar. Chem. **8:** 167–188.

JØRGENSEN, B. B., AND D. J. DES MARAIS. 1990. The diffusive boundary layer of sediments: Oxygen microgradients over a microbial mat. Limnol. Oceanogr. **35:** 1343–1355.

———, AND N. P. REVSBECH. 1983.Colorless sulfur bacteria, *Beggiatoa* spp. and *Thiovulum* spp., in O_2 and H_2S microgradients. Appl. Environ. Microbiol. **45:** 1261–1270.

KOMADA, T. 1996. Verification of the use of pH and pCO_2 microelectrodes in determining the concentration gradients of total CO_2 in marine sediments. M.S. thesis, Rutgers Univ.

LI, Y. H., AND S. GREGORY. 1974. Diffusion of ions in sea water and in deep-sea sediments. Geochim. Cosmochim. Acta **38:** 703–713.

MCCAFFREY, R. J., AND OTHERS. 1980. The relation between pore-water chemistry and benthic fluxes of nutrients and manganese in Narragansett Bay, Rhode Island. Limnol. Oceanogr. **25:** 31–44.

MCDUFF, E., AND R. A. ELLIS. 1979. Determining diffusion coefficients in marine sediments: A laboratory study of the validity of resistivity techniques. Am. J. Sci. **279:** 666–675.

MILLER, J. C., AND J. N. MILLER. 1984. Statistics for analytical chemistry. Wiley.

MILLERO, F. J. 1995. Thermodynamics of the carbon dioxide system in the oceans. Geochim. Cosmochim. Acta **59:** 661–677.

RAICH, J. W., AND C. S. POTTER. 1995. Global patterns of carbon dioxide emissions from soils. Global Biogeochem. Cycles **9:** 23–36.

RASMUSSEN, H., AND B. B. JØRGENSEN. 1992. Microelectrode studies of seasonal oxygen uptake in a coastal sediment: Role of molecular diffusion. Mar. Ecol. Prog. Ser. **81:** 289–303.

REIMERS, C. E., K. M. FISCHER, R. MEREWETHER, K. L. SMITH, AND R. A. JAHNKE. 1986. Oxygen microprofiles measured in situ in deep ocean sediments. Nature **320:** 741–744.

———, R. A. JAHNKE, AND D. C. MCCORKLE. 1992. Carbon fluxes and burial rates over the continental slope and rise off central California with implications for the global carbon cycle. Global Biogeochem. Cycles **6:** 199–224.

———, AND K. L. SMITH, JR. 1986. Reconciling measured and predicted fluxes of oxygen across the deep sea sediment–water interface. Limnol. Oceanogr. **31:** 305–318.

REVSBECH, N. P. 1989. Diffusion characteristics of microbial communities determined by use of oxygen microsensors. J. Microbiol. Methods **9:** 111–122.

———, AND B. B. JØRGENSEN. 1986. Microelectrodes: Their use in microbial ecology, p. 293–352. *In* K. C. Marshall [ed.], Advances in microbial ecology. Plenum.

———, AND D. M. WARD. 1983. Oxygen microelectrode that is insensitive to medium chemical composition: Use in an acid microbial mat dominated by *Cyanidium caldarium.* Appl. Environ. Microbiol. **45:** 755–759.

ROY, R. N., AND OTHERS. 1993. Determination of the ionization constants of carbonic acid in sea water. Mar. Chem. **44:** 249–268.

RUTGERS VAN DER LOEFF, M. M., L. G. ANDERSON, P. O. J. HALL, Å. IVERFELDT, A. B. JOSEFSON, B. SUNDBY, AND S. F. G. WESTERLUND. 1984. The asphyxiation technique: An approach to distinguishing between molecular diffusion and biologically mediated transport at the sediment–water interface. Limnol. Oceanogr. **29:** 675–686.

SMITH, R. M., AND A. E. MARTELL. 1976. Critical stability constants, v. 4: Inorganic ligands. Plenum.

STUMM, W., AND J. J. MORGAN. 1981. Aquatic chemistry, 2nd ed. Wiley.

SZEDLMAYER, S. T., AND K. W. ABLE. 1993. Ultrasonic telemetry of age-0 summer flounder, *Paralichthys dentatus,* movements in a southern New Jersey estuary. Copeia **3:** 728–736.

ULLMAN, W. J., AND R. C. ALLER. 1982. Diffusion coefficients in nearshore marine sediments. Limnol. Oceanogr. **27:** 552–556.

WEISS, R. F. 1974. Carbon dioxide in water and seawater: The solubility of a non-ideal gas. Mar. Chem. **2:** 203–215.

ZHAO, P., AND W.-J. CAI. 1997. An improved potentiometric pCO_2 microelectrode. Anal. Chem. **69:** 5052–5058.

Received: 20 February 1997
Accepted: 28 May 1998